

Article

Characterisation of Bovine Amniotic Membrane with Hydroxyapatite Bio-Composite

Octarina ^{1,2}, Elly Munadzirah ^{3,*}, Fathilah Abdul Razak ⁴ and Meircurius Dwi Condro Surboyo ⁵¹ Doctoral Program, Faculty of Dental Medicine, Universitas Airlangga, Surabaya 60132, Indonesia² Department of Dental Material, Faculty of Dentistry, Universitas Trisakti, Jakarta 11440, Indonesia³ Department of Dental Material, Faculty of Dental Medicine, Universitas Airlangga, Surabaya 60132, Indonesia⁴ Department of Oral and Craniofacial Sciences, Faculty of Dentistry, Universiti Malaya, Kuala Lumpur 50603, Malaysia⁵ Department of Oral Medicine, Faculty of Dental Medicine, Universitas Airlangga, Surabaya 60132, Indonesia

* Correspondence: elly-m@fkg.unair.ac.id

Abstract: The fabrication of bio-composite-derived bovine amniotic membrane (BAM) with hydroxyapatite (HAp) is an approach to combining organic and inorganic bio-material to improve the properties of both materials. This research aims to combine, fabricate and characterise the bio-composite of BAM–HA. The combination of bio-composite is made from BAM and HAp in a ratio of 30:70, 35:65, and 40:60. Dried BAM is immersed in saline and then blended until it forms an amniotic slurry with a jelly-like consistency. At this stage, HAp is added so that it can bind to BAM. After the mixture is homogeneous, the freeze-drying process is carried out. After fabrication, all the bio-composites were characterised using Fourier transform infrared spectrometry (FTIR), X-ray diffraction (XRD), scanning electron microscopy (SEM) and porosity analysis, and biological activity was conducted using fibroblasts. The bio-composite has functional groups of amides I, II, III, A, B, OH, CO₃²⁻ and PO₄³⁻ according to the results of the FTIR. The XRD analysis showed the presence of HAP crystals. This functional group and the crystal HAP indicate that these two materials are bound. An SEM examination revealed a variety of porous patterns on the surface area. The bio-composite with BAM and HAp at a ratio of 35:65 has a higher mean pore size of 155.625 μm with mean porosity of 89.23% and can maintain the fibroblast viability of 95.14%. In conclusion, the study successfully combined both bio-materials BAM and HAp, which have potential synergistic effects on soft and hard tissue regeneration. The ratio of 35:65 showed good characteristics and was non-toxic.

Keywords: bovine amnion; hydroxyapatite; bio-composite; fabrication; characterisation**Citation:** Octarina; Munadzirah, E.; Razak, F.A.; Surboyo, M.D.C.Characterisation of Bovine Amniotic Membrane with Hydroxyapatite Bio-Composite. *Coatings* **2022**, *12*, 1403. <https://doi.org/10.3390/coatings12101403>

Academic Editor: Roman A. Surmenev

Received: 11 August 2022

Accepted: 22 September 2022

Published: 26 September 2022

Publisher's Note: MDPI stays neutral with regard to jurisdictional claims in published maps and institutional affiliations.**Copyright:** © 2022 by the authors. Licensee MDPI, Basel, Switzerland. This article is an open access article distributed under the terms and conditions of the Creative Commons Attribution (CC BY) license (<https://creativecommons.org/licenses/by/4.0/>).

1. Introduction

Bovine amniotic membrane (BAM) is a bio-material that comes from the bovine innermost layer of the foetus placenta that contains structural proteins and biologically active factors [1]. This bio-material has similarities with the human amniotic membrane with its unique structure and its physical and biological properties, making it useful as a bio-material in regenerative medicine [2]. The growth factors present in this membrane consist of epidermal growth factors (EGF), transforming growth factor- α (TGF- α), keratinocytes growth factors (KGF), hepatocytes growth factors (HGF), basic fibroblast growth factors (bFGF) and transforming growth factors β (TGF- β) [3]. The extracellular matrix of the amniotic membrane consists of collagen types I, III, IV, V, VI and XV; laminin; nidogen; fibronectin; and proteoglycans [4]. This collagen will potentially be bio-medical material in tissue engineering [5]. In addition, the amniotic membrane shows an osteoinductive ability during bone formation [6].

A limitation of the amniotic membrane is that it is easily biodegradable, making it difficult to maintain the structural integrity required for bone regeneration [7]. Easy bio-degradation occurs because the collagen content in the amniotic membrane is easily

absorbed [8]. This bio-degradation causes bone healing only in the marginal area, making it less effective at reducing resorption from alveolar bone [9]. Combining amniotic membrane and osteoconductive bone-forming material will increase bone regeneration [10]. The amniotic membrane should be combined with mineral calcium salts (Ca^{2+}) to improve the structure and enhance osteogenesis. Calcium salts are the main component of hydroxyapatite [11,12].

Hydroxyapatite (HAp) ($\text{Ca}_{10}(\text{PO}_4)_6(\text{OH})_2$) is the most stable calcium phosphate salt. This material plays a role in bone formation or bone substitution [13]. HAp from bovine has a chemical composition similar to human bone. It is constituted by carbonates (CO_3^{2-}), sodium (Na^+), magnesium (Mg^{2+}), iron (Fe^{2+}), fluoride (F^-), silicates and chlorides (Cl^-). This composition will affect various bio-mechanical reactions associated with bone metabolism [14]. In addition to being bio-compatible, HAp bovine has osteoconductive ability and stimulates osteoblast differentiation [15]. However, this osteoconductive ability causes the HAp to not be well absorbed in the extraction socket. If HAp is not well absorbed, it will cause inflammation and the healing and formation of alveolar bone to be delayed.

Bone mass is a composite that consists of 20%–30% organic matrix, 60%–70% inorganic fraction, and 10% water [16]. Alveolar bone has almost the same composition as cementum [17]. The composition comprises 65% HAp mineral and an additional 35% collagen organic matrix [18]. This study aims to combine the two materials, namely BAM with HAp, to improve the properties of both materials. Based on this ratio, in this study, bio-composites were fabricated by a combination of BAM–HAp in different ratios: 30:70, 35:65 and 40:60. Both BAM and HAp, are natural bio-materials derived from the waste of bovine. However, these two bio-materials are expected to have great potential synergism for wound healing and bone tissue. In the development process of novel bio-composites, it is crucial to conduct a full set of physicochemical characterisation tests before conducting *in vitro* and further *in vivo* tests.

Material characterisation provides information about the physical and chemical properties of the material that can be influenced by the size and components [19]. In this study, a characterisation test will be carried out using Fourier transform infrared (FTIR) to analyse functional groups of bio-materials [20]; X-ray diffraction (XRD) to study the crystal structure of a material by using X-rays [21]; scanning electron microscope (SEM) to analyse the shape of the surface, topography, morphology and composition of a material [22]; and porosity analysis to study the pore structure of materials that are suitable for cells to grow and develop [23].

2. Materials and Methods

2.1. Fabrication of Materials

2.1.1. BAM Preparation

BAM–HAp material was fabricated at the Bio-material Center Installation of the Network Bank RSUD Dr Soetomo. Fresh BAM came from female bovines from farms in Malang, East Java. First, the BAM was immersed with NaCl 0.05% solution for 10 min. After that, it was re-washed with distilled water until the NaCl solution was clean. The chorion of the BAM was separated, then cleaned of blood clots and washed with aqua dest. After that, the clean BAM was stretched on a sheet covered with gauze. The BAM was put in the freezer at $-80\text{ }^\circ\text{C}$ for $1 \times 24\text{ h}$, then freeze-dried for $1 \times 24\text{ h}$ at $-100\text{ }^\circ\text{C}$ to make a dried BAM.

2.1.2. HAp Preparation

The cancellous bone was cut into small pieces and washed with H_2O_2 . After that, the fat was removed at a temperature of $60\text{ }^\circ\text{C}$ in an ultrasonic shaker. Washing with distilled water was carried out to remove H_2O_2 . Afterwards, the bones were dried at room temperature to minimise the moisture content. Next was the roasting process with a furnace at $1000\text{ }^\circ\text{C}$ for one hour. After that, it was rinsed with distilled water. It was then

dried again in the oven at a temperature of 60–100 °C. When completely dry, it was ground with a bone miller until particles formed. A sieving machine separated the HAp particles with a size of 150 µm.

2.1.3. Bio-Composite Fabrication

The bio-composite in this study was fabricated with four types based on ratios of BAM and Hap: the BAM–HAp 30:70, BAM–HAp 35:65, BAM–HAp 40:60 and modified BAM as a control group. First, dried BAM and HAp powder were prepared by weight ratio unit, respectively, for each ratio sample of 3 g:7 g; 3.5 g:6.5 g; 4 g:6 g; and for the control group (modified BAM) 3 g BAM.

Then, the BAM was cut into pieces of about 2 cm and added with 40 mL of 0.9% NaCl. The existing BAM was soaked for 5 min until it absorbed the liquid. After that, it was mashed using a blender for about 10 min to produce an amniotic slurry. The amniotic slurry was then added to the HAp powder. In the control group, HAp was not added. The composite material was then stirred until it formed a homogeneous mixture and put into a petri dish with a diameter of 1 cm. After that, it was put in the freezer (Thermo, Waltham, MA, USA) at $-80\text{ }^{\circ}\text{C}$ for $1 \times 24\text{ h}$. Then, the sample was placed for freeze-drying (Thermo drying VirTis, USA) for $1 \times 24\text{ h}$ at $-100\text{ }^{\circ}\text{C}$. It was then sterilised with 25 kGy gamma rays. The final result of this sample will be in the form of a sponge (Figure 1).

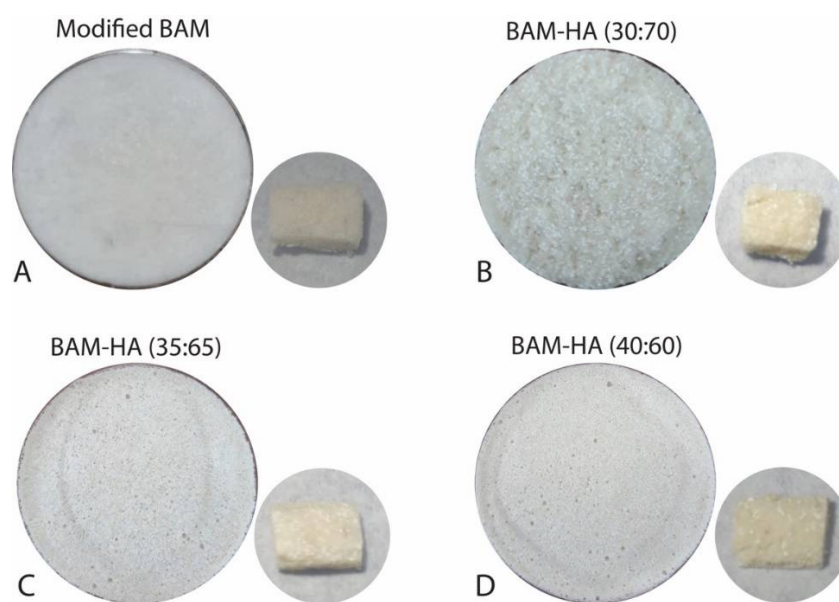


Figure 1. The bio-composite BAM–HAp with different ratios. (A) Modified BAM; (B) 30:70; (C) 35:65; (D) 40:60.

2.2. Physicochemical Characterization

2.2.1. FTIR Analysis

The sample was added with potassium bromide (Sigma–Aldrich, Saint Louis, MO, USA) in a ratio of 1:4. The mixture was put in a mortar and pounded with a pestle until homogeneous. After this, the homogeneous mixture was put in a pan with a diameter of 4 mm. FTIR analysis was conducted using IR Prestige-21 (Shimadzu, Kyoto, Japan) in $400\text{--}4000\text{ cm}^{-1}$ and 2.0 cm^{-1} resolutions and transmittance percentage mode. The results of the FTIR analysis were displayed in graphic form and adjusted to the existing database with Origin Pro software (OriginLab Corporation, Northampton, MA, USA).

2.2.2. XRD Analysis

Samples were cut with a thickness of 1–3 mm with a length and width of $3\text{ mm} \times 3\text{ mm}$. The analysis used a Bruker D8 XRD machine (Denmark, Nordic) with a scan range of

10–90° with a speed of 0.1 s per step. The results of the XRD analysis were displayed in graphic form and adjusted to the existing database with X'pert and Origin Pro software (OriginLab Corporation, Northampton, MA, USA).

2.2.3. SEM Analysis

Samples were prepared in a size of 1 cm × 1 cm. The sample was then coated with gold (fine coater JFC 1600) before testing. The sample was then vacuumed in high vacuum mode with a 15 kV SEI to be analysed with SEM (JEOL, JSM 6510-LA, Tokyo, Japan). Magnifications were set at 50× and 500×, and then the surface morphology of the pores, pore size and porous shape were analysed with Image-J.

2.2.4. Porosity Analysis

Samples were prepared with a size of 0.2 cm × 0.2 cm × 0.7 cm in the form of a cube. The initial volume (V0) of the sample was calculated and the initial weight of the BAM–HAp sample (W0) was weighed on an analytical balance (Fujitsu, Tokyo, Japan). The sample was then immersed in absolute ethanol until saturated. After that, the sample was re-weighed as the final weight (W1) with an analytical balance (Fujitsu, Japan). Then, it was calculated using the formula:

$$\text{porosity (\%)} = \frac{[W1 - W0] \times 100\%}{V0} \quad (1)$$

2.2.5. Biological Activity Using Fibroblasts

Fibroblast cells were taken from BHK-21 cell cultures. The cells were planted in Eagle's minimum essential medium (MEM) containing 10% serum foetal bovine (FBS) and then incubated for 24 h at a temperature of 37 °C. Cells were transferred into roux vials with a density of 2×10^5 cells/mL.

The MTT assay was performed to assess the ability of the bio-composites to maintain the fibroblast viability. The 50 µL Eagle's MEM and 50 µL fibroblast cells were put in wells, followed by each type of bio-composite (0.1 mg). The control media contained 50 µL Eagle's MEM, and the control cell contained 50 µL Eagle's MEM and 50 µL fibroblast cells. MTT dissolved in PBS 5 mg/mL was then added to each well containing 10 µL of media, then re-incubated for approximately 4 h at a temperature of 37 °C. The viability of fibroblasts was then measured based on absorbance using spectrophotometry with a wavelength of 620 nm. The viability of fibroblast was calculated with the formula [24]:

$$\text{viability (\%)} = \frac{[\text{OD test} - \text{OD control media}] \times 100\%}{\text{OD control cell} + \text{OD control media}} \quad (2)$$

The differences in porosity and fibroblast between each bio-composite were analysed using one-way ANOVA with post hoc Gomes Howell test with the *p*-value as *p* < 0.01. The analysis used was an IBM SPSS Statistic for Mac version 26.

3. Results

3.1. FTIR Analysis

All of the three-sample bio-composite types in FTIR analysis have the absorption of the infrared waves resembling the BAM modification (control). Therefore, the bio-composite has the same functional groups as the control sample, namely the amide I, II, III, A, B and OH. However, the FTIR chart of modified BAM does not show HAp functional groups, PO_4^{3-} and CO_3^{2-} , as found in the samples of all bio-composite types. These functional groups do not appear in the modified BAM (Figure 2).

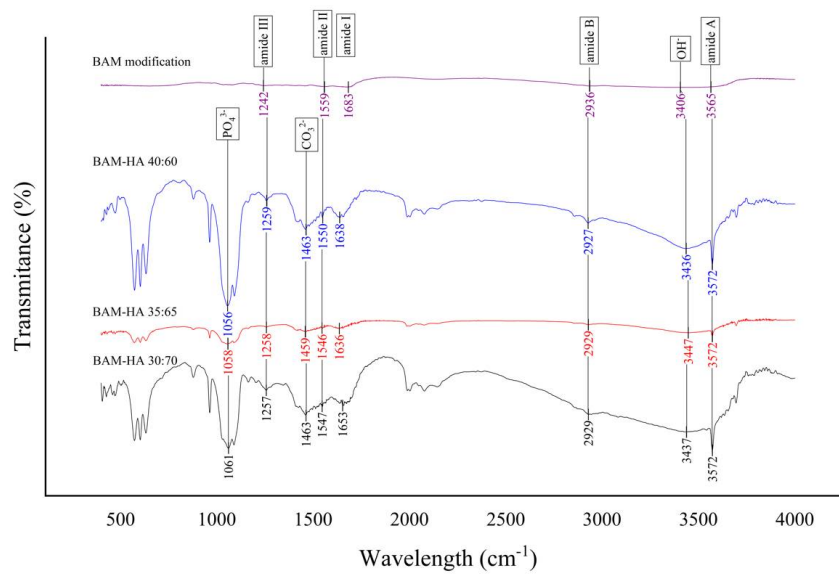


Figure 2. The result of FTIR analysis of all types of bio-composite and modified BAM.

3.2. XRD Analysis

The most significant diffraction peaks of HAp according to XRD analyses were identified, respectively, at 36.9° 2θ, 37.2° 2θ and 37° 2θ in all types of bio-composites. HAp crystal diameters of these samples were 1040 nm, 868 nm and 867 nm based on Scherrer’s calculations, while HAp crystallinity levels were 19%, 28% and 34%, subsequently. There is a sharp peak in the graphic findings of the modified BAM sample, but it does not exhibit a peak that represents the HAp crystal reference pattern (Figure 3). The HAp crystal has peaks at 12.6°; 19.8°; 21.8°; 25.3°; 26.5°; 29.5°; 30.1°; 32.8°; 33.7°; 37°; 37.5°; 38.4°; 39.8°; 41.5°; 44.6°; 45.8°; 46.5°; 47.3°; 49.1°; 49.6°; 51.4°; 52°; 53.2°; 53.3°; 54.8°; 56.4°; 57°; 58.1°; 59.3°; 60.3°; 61.3°; 62.6°; 64.1°; 65.9°; 66.5°; 67.4°; 68.4°; 68.7°; 68.8°; 69.7°; 70.8°; 71.4°; 72.8°; 73.1°; 74.6°; 75.2°; 75.9°; 76.1°; 77.1°; 78.9°; 80.1°; 81.6°; 82.2°; 82.4°; 83.1°; 83.6°; 84.5°; 85.2°; 85.5°; 85.7°; 86.3°; 86.7°; 87.2°; 88.2°; 88.6°; and 89.8° 2θ according to the International Center for Diffraction Data (ICCD®).

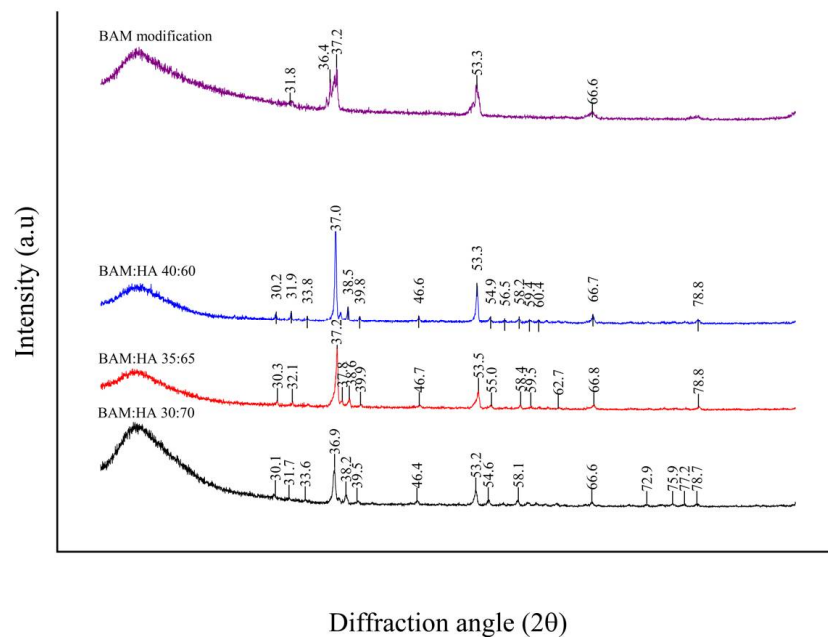


Figure 3. Graph of XRD analysis of all types of bio-composite and modified BAM.

3.3. SEM Analysis

Modified BAM and bio-composite (40:60) show nearly identical surfaces. On the surfaces in these two samples, the pores are evenly distributed and spread with almost the same size (Figure 4a,b). The higher HAp content makes a larger porous size and reduces the number and irregularity of the pores. The surface also looks denser, as seen in other types of bio-composites (35:65 and 30:70) (Figure 4c,d).

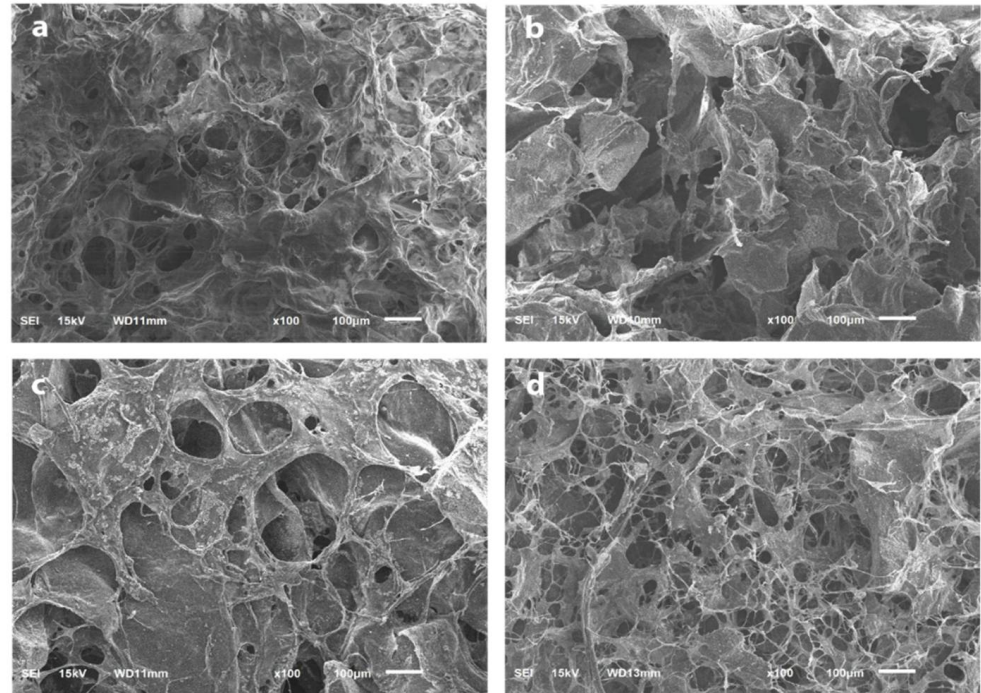


Figure 4. The surface and porosity analysis using SEM with 100× magnification. (a) Modified BAM; (b) bio-composite (30:70); (c) bio-composite (35:65); (d) bio-composite (40:60).

3.4. Porosity

The bio-composites (40:60) and modified BAM have more pores with smaller pore sizes. On the other hand, the other bio-composites (30:70 and 35:65), which contained more Hap, have fewer pores with a larger pore size (Table 1). As a result, the modified BAM and bio-composites (40:60) have higher porosity compared to the other bio-composite, respectively, $(105.93\% \pm 3.81\%)$ and $(103.25\% \pm 9.50\%)$. Meanwhile, the bio-composite (30:70) has the lowest porosity $(76.89\% \pm 6.15\%)$ (Figure 5).

Table 1. The pores size and porosity of modified BAM and all types of bio-composites.

Group	Pore Size (μm)			Porosity (%)	
	Mean	Minimum	Maximum	Mean \pm SD	<i>p</i>
modified BAM	89.09	208.25	14.13	105.93 ± 3.81	0.0001
bio-composite (30:70)	153.02	420.44	37.99	76.89 ± 6.15	
bio-composite (35:65)	155.62	316.10	43.39	89.23 ± 7.51	
bio-composite (40:60)	72.424	279.89	20.51	103.25 ± 9.50	

SD: standard deviation.

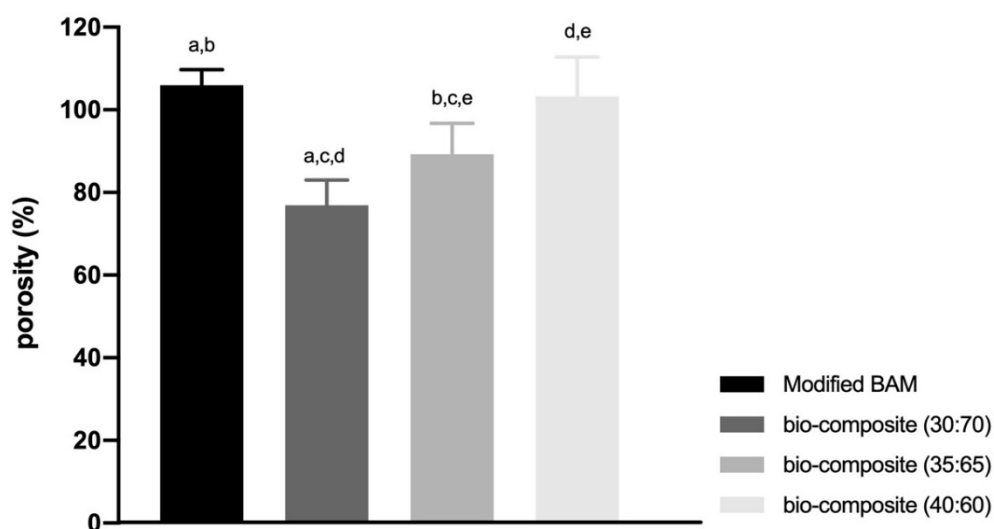


Figure 5. The result of porosity percentage of all types of bio-composite and modified BAM. (a–e means significant difference in each group with the Gomes Howell test with p -value as $p < 0.01$).

3.5. Viability of Fibroblast Cells

The bio-composite (ratio 30:70) has the highest fibroblast viability (98.14%) among other types of bio-composites. The bio-composite (ratio 40:60) has higher fibroblast viability than bio-composites (ratio 35:65) (96.89% and 95.14%, respectively) (Table 2).

Table 2. The fibroblast viability of modified BAM and all types of bio-composites.

Group	Mean \pm SD OD	Viability (%)	p -Value
Control media	0.0670 \pm 0.0088	0	
Control cells	0.5080 \pm 0.0592	100	
bio-composite (30:70)	0.4998 \pm 0.0483	98.14	0.860
bio-composite (35:65)	0.4866 \pm 0.0507	95.14	
bio-composite (40:60)	0.4943 \pm 0.0541	96.89	

SD: standard deviation; OD: optical density; p -value obtained from one-way ANOVA.

4. Discussion

In this study, preparation of BAM and HAp in dry form was carried out to balance the ratio in terms of weight. BAM in dry condition was cut into pieces and immersed in NaCl to facilitate softening [11]. NaCl as an organic solvent was used to facilitate BAM refining with a blender. BAM was blended to form an amniotic slurry-like jelly during this procedure. Next, the addition of HAp was carried out to create a bond between BAM and HAp. BAM acts as a matrix in this bio-composite fabrication, and HAp acts as a filler [25]. In the research, particles with 150 μ m used in the study more easily incorporated and bonded with BAM. Bigger or smaller particle sizes of HAp made fragile bio-composite.

Bone tissue is a bio-composite. Therefore, the fabrication of this material is expected to be a bio-composite bone replacement [16]. In this study, bio-composite was made into different ratios similar to bone structure. Bone, or dentin, has a ratio of organic and inorganic components of 30:70 [26]. Alveolar bone or cementum has an organic and inorganic component composition of 35:65 [18]. On the other hand, bio-composite (40:60) with a more organic matrix of as much as 40% was made to increase the scaffold absorption for wound healing [27]. The fabrication of this bio-composite modifies the properties of the material. In addition, bio-composite material is also expected to act as a scaffold for the formation of new bone or as a drug carrier and distribute it directly to bone [28].

In the results of the FTIR analysis, all types of bio-composite and modified BAM have amide functional groups I, II, III, A, B and OH. Amide is a chemical compound by a

functional group $RnE(O) \times NR'2$ (R and R' refer to H or organic groups). The functional groups of amides I, II, III, A, B and OH are characterised by O-H, N-H, C-H and N-H bonds, which indicate the presence of collagen [29,30]. All types of bio-composites showed the presence of PO_4^{3-} and CO_3^{2-} functional groups. The functional groups PO_4^{3-} and CO_3^{2-} are parameters of HAp which are characterised by O-P-O, C-O and Ca-O bonds. The modified BAM sample did not show any PO_4^{3-} and CO_3^{2-} functional groups due to uncontained HAp during the fabrication [31,32].

The presence of amide and hydroxyapatite functional groups in the bio-composite indicates that BAM's incorporation with HAp can be carried out and has been successful. The FTIR results also showed no change in the functional group of the amide absorption peak in the modified BAM and bio-composite. Furthermore, research by Chen et al., 2017, analysed collagen scaffolds with HAp and showed the same functional groups between collagen scaffolds and combined collagen-HAp scaffolds [33].

The protein spectrum is characterised by stretching and bending vibrations of the amide functional group. In this study, the bio-composite and modified BAM did not show any shift in the peaks of the amide I and II functional groups. These functional group peaks show that the collagen in the bio-composite did not undergo denaturation during the fabrication process [12,34].

The XRD of all types of bio-composites found sharp diffraction peaks from X-rays that indicate the presence of HAp crystals. According to the references from The International Centre for Diffraction Data (ICDD[®]) Powder Diffraction FileTM (PDF[®]) (No. 01-073-0294), the bio-composites showed HAp crystals with the chemical formula $Ca_5(PO_4)_3OH$ with the HAp diffraction peaks shown in Figure 3 [35].

According to the XRD analysis, high and sharp graph peaks indicate the abundance of HAp crystals. Bio-composite (35:65) has a microcrystal size and a low degree of crystallisation. The micro-sized crystals can improve osteogenic potential by promoting cell adhesion, dissemination and proliferation [36]. These crystals with a size of $<2-3 \mu m$ and a low degree of crystallinity are the best material to promote healing [37].

In this study, SEM analysis showed the presence of micro-sized pores on the sample's surface. The freeze-drying process caused the formation of pores during sample fabrication. In addition, the freeze-drying process removes the liquid in the sample by sublimation so that it does not remove its main components and produces a micro-porous structure in the sample [38]. This study found that those with the highest BAM content would have more pores with smaller sizes. The higher pore formation was found in the modified BAM and bio-composite (40:60), where BAM contained collagen. Collagen is an organic substance that has much fluid. Therefore, during the freeze-drying process, it will leave the most micro-pores. Freeze-dried collagen will create a micro-structure ranging $20-40 \mu m$ [39]. Varying pore size and reduced pore number were shown by SEM images on bio-composites (35:65 and 30:70). The higher the HAp content, the smaller the number of pores and the more irregular the shape of the pores. HAp also makes the material denser and more brittle [40].

Pore size is essential for cell growth and nutrient diffusion, thus facilitating cell attachment and vascularisation. In addition, the pores are a fundamental parameter for the transport of oxygen and nutrients from the extracellular matrix to the interior of the scaffold. The pore size was observed to be in the range of $100-300 \mu m$. This pore size is suitable for tissue engineering applications [41]. Scaffold porosity, pore size and overall pore structure affect tissue formation and infiltration into the bio-material construction. In this study, the pore size was calculated with Image-J. Image-J is software that accelerates the analysis images by automatically quantifying the pore size area. The pore size of the sample suitable for osteoconduction and soft tissue regeneration in this study was bio-composite (35:65). The optimum pore size for osteoconduction ranges $200-350 \mu m$, and soft tissue regeneration ranges $20-125 \mu m$. This optimum pore size will affect and improve tissue regeneration [42].

In this study, the lowest mean percentage of porosity owned by bio-composite (30:70) was $(76.89\% \pm 6.15\%)$. In bio-materials with a porosity percentage of 70%, the present porosity presentation cannot support growth and attachment cells in the early stages, so cell proliferation is inhibited. Inhibited cell proliferation causes tissue healing to be obstructed [43]. The highest mean porosity percentage belonged to the modified BAM sample $(105.93\% \pm 3.81\%)$ and bio-composite (40:60) $(103.25\% \pm 9.50\%)$. A higher rate of porosity will increase nutrient absorption and hydraulic permeability. However, the stiffness will be lower, which will cause a loss of mechanical properties, and the material will become easily degraded [44]. Bio-materials with a large percentage of porosity cause a smaller surface area so that fewer cells adhere and will inhibit cell proliferation [45]. Bio-composites ideal porosity percentage was 35:65 $(89.23\% \pm 7.51\%)$. The ideal porosity percentage for bone healing is in the range of 80%–90%. This percentage of porosity will cause a larger surface area for bio-material, which is more favourable for early cell attachment [23,46].

The viability of fibroblasts is performed to determine the toxicity of the bio-composite. Material can be referred to as non-toxic if the viability is more than 70%. The reduction of cell viability by more than 30% is considered a cytotoxic effect based on ISO standard 10993-5. In all other types of bio-composites, it was found that the viability of fibroblasts was above 90%. Bio-composite (35:65) produces the highest viability fibroblast, which is 98.14%. From these results, it can be concluded that all bio-composites are not toxic and can be proposed as materials for bone regeneration, especially in the field of dentistry.

5. Conclusions

In conclusion, the fabrication of bio-composites combining BAM and HAp with varied ratios of 30:70, 35:65 and 40:60 was successfully carried out. Analysis of FTIR and XRD showed that the BAM and HAp could bond with each other. SEM results and porosity characteristic tests showed that bio-composite (35:65) has good characteristics and a viability of 95.14%.

Author Contributions: Conceptualisation, E.M. and O.; methodology, E.M. and O.; software, E.M. and O.; validation, E.M.; formal analysis, O.; investigation, E.M. and O.; data curation, E.M. and O.; writing—original draft preparation, O.; writing—review and editing, M.D.C.S. and F.A.R.; visualisation, O., E.M. and M.D.C.S.; supervision, E.M.; project administration, E.M.; funding acquisition, E.M. and O. All authors have read and agreed to the published version of the manuscript.

Funding: This research received funding from the Ministry of Education and Culture with grant number 847/UN3.15/PT/2022.

Institutional Review Board Statement: The study was conducted in accordance with the Declaration of Helsinki and approved by the Institutional Review Board in the Faculty of Dental Medicine. Universitas Airlangga with registration number 360/HRECC.FODM/VII/2021.

Informed Consent Statement: Not applicable.

Data Availability Statement: Not applicable.

Acknowledgments: The authors would like to thank The Tissue Bank Centre, Surabaya for supporting the process of fabrication of bio-composite and Pascal Filio for supporting during XRD analysis.

Conflicts of Interest: The authors declare no conflict of interest.

References

1. Singh, M.; Madhan, G. Comparison of ability of platelet-rich fibrin vs collaplug in maintaining the buccal bone height of sockets following extractions in 20 patients. *J. Health Sci. Res.* **2017**, *8*, 1–6.
2. Siswanto, R.; Rizkawati, D.M.; Ifada, A.A.; Putra, A.P.; Rachmayani, F.; Widiyanti, P. Bovine freeze dried amniotic membrane (FD-AM) covered sterile gauze for wound dressing. *Asian Acad. Soc. Int. Conf. Proc. Ser.* **2013**, 68–71.
3. Koizumi, N.; Inatomi, T.; Sotozono, C.; Fullwood, N.J.; Quantock, A.J.; Kinoshita, S. Growth factor mRNA and protein in preserved human amniotic membrane. *Curr. Eye. Res.* **2000**, *20*, 173–177. [[CrossRef](#)]

4. Niknejad, H.; Peirovi, H.; Jorjani, M.; Ahmadiani, A.; Ghanavi, J.; Seifalian, A.M. Properties of the amniotic membrane for potential use in tissue engineering. *Eur. Cells Mater.* **2008**, *15*, 88–99. [[CrossRef](#)]
5. Gunasekaran, D.; Thada, R.; Jeyakumar, G.F.S.; Manimegalai, N.P.; Shanmugam, G.; Sivagnanam, U.T. International Journal of Biological Macromolecules Physicochemical characterization and self-assembly of human amniotic membrane and umbilical cord collagen: A comparative study. *Int. J. Biol. Macromol.* **2020**, *165*, 2920–2933. [[CrossRef](#)]
6. Tang, K.; Wu, J.; Xiong, Z.; Ji, Y.; Sun, T. Human acellular amniotic membrane: A potential osteoinductive biomaterial for bone regeneration. *J. Biomater. Appl.* **2017**, *32*, 754–764. [[CrossRef](#)]
7. Dimitriou, R.; Mataliotakis, G.I.; Calori, G.M.; Giannoudis, P.V. The role of barrier membranes for guided bone regeneration and restoration of large bone defects: Current experimental and clinical evidence. *BMC Med.* **2012**, *10*, 81. [[CrossRef](#)] [[PubMed](#)]
8. Castro-ceseña, A.B.; Camacho-villegas, T. Effect of starch on the mechanical and in vitro properties of collagen-hydroxyapatite sponges for applications in dentistry. *Carbohydr. Polym.* **2016**, *148*, 78–85. [[CrossRef](#)]
9. Fickl, S.; Zuh, O.; Wachtel, H.; Stappert, C.F.J.; Stein, J.M.; Hürzeler, M.B. Dimensional changes of the alveolar ridge contour after different socket preservation techniques. *J. Clin. Periodontol.* **2008**, *35*, 906–913. [[CrossRef](#)]
10. Starecki, M.; Schwartz, J.A.; Grande, D.A. Evaluation of amniotic-derived membrane biomaterial as an adjunct for repair of critical sized bone defects. *Adv. Orthop. Surg.* **2014**, *2014*, 72586. [[CrossRef](#)]
11. Dewey, M.J.; Johnson, E.M.; Slater, S.T.; Milner, D.J.; Wheeler, M.B.; Harley, B.A.C. Mineralized collagen scaffolds fabricated with amniotic membrane matrix increase osteogenesis under inflammatory conditions. *Regen. Biomater.* **2020**, *7*, 247–258. [[CrossRef](#)]
12. Sabouri, L.; Farzin, A.; Kabiri, A.; Milan, P.B.; Farahbakhsh, M.; Mehdizadehkashi, A.; Kajbafzadeh, A.; Samadikuchaksaraei, A.; Yousefbeyk, F.; Azami, M.; et al. Mineralized human amniotic membrane as a biomimetic scaffold for hard tissue engineering applications. *ACS Biomater. Sci. Eng.* **2020**, *6*, 6285–6298. [[CrossRef](#)]
13. Machtei, E.E.; Mayer, Y.; Horwitz, J.; Zigdon-Giladi, H. Prospective randomized controlled clinical trial to compare hard tissue changes following socket preservation using alloplasts, xenografts vs no grafting: Clinical and histological findings. *Clin. Implant Dent. Relat. Res.* **2019**, *21*, 14–20. [[CrossRef](#)]
14. Ratnayake, J.T.B.; Gould, M.L.; Shavandi, A.; Mucalo, M.; Dias, G.J. Development and characterization of a xenograft material from New Zealand sourced bovine cancellous bone. *J. Biomed. Mater. Res. B Appl. Biomater.* **2017**, *105*, 1054–1062. [[CrossRef](#)]
15. Mozartha, M. Hidroksiapatit dan aplikasinya di bidang kedokteran gigi. *J. Vis. Lang. Comput.* **2015**, *11*, 287–301.
16. Kołodziejaska, B.; Kaflak, A.; Kolmas, J. Biologically inspired collagen/apatite composite biomaterials for potential use in bone tissue regeneration—A review. *Materials* **2020**, *13*, 1748. [[CrossRef](#)]
17. Shahmoradi, M.; Bertassoni, L.E.; Elfallah, H.M.; Swain, M. *Fundamental Structure and Properties of Enamel, Dentin and Cementum*; Springer: Berlin/Heidelberg, Germany, 2014; pp. 511–547.
18. Oosterlaken, B.M.; Vena, M.P.; de With, G. In Vitro mineralization of collagen. *Adv. Mater.* **2021**, *33*, 2004418. [[CrossRef](#)]
19. Abdullah, M.; Khairurrijal, K. Review: Karakterisasi nanomaterial. *J. Nanosains Nanoteknologi.* **2009**, *2*, 1–9.
20. Nandiyanto, A.B.D.; Oktiani, R.; Ragadhita, R. How to read and interpret FTIR spectroscopy of organic material. *Indones. J. Sci. Technol.* **2019**, *4*, 97–118. [[CrossRef](#)]
21. Scimeca, M.; Bischetti, S.; Lamsira, H.K.; Bonfiglio, R.; Bonanno, E. Energy Dispersive X-ray (EDX) microanalysis: A powerful tool in biomedical research and diagnosis. *Eur. J. Histochem.* **2018**, *62*, 2841. [[CrossRef](#)]
22. Choudhary, O.P.; Husbandry, A.; Choudhary, P. Scanning electron microscope: Advantages and disadvantages in imaging scanning electron microscope: Advantages and disadvantages in imaging components. *Int. J. Curr. Microbiol. Appl. Sci.* **2017**, *85*, 1–7.
23. El Milla, L.; Indrani, D.J.; Irawan, B. Sintesis dan uji porositas scaffold hidroksiapatit/alginat. *ODONTO Dent. J.* **2018**, *5*, 49. [[CrossRef](#)]
24. Surboyo, M.D.C.; Mahdani, F.Y.; Ayuningtyas, N.F.; Santosh, A.B.R.; Ernawati, D.S.; Mansur, D.; Arundina, I.; Nagoro, A.A.B.; Rahmadhany, I.P. The cytotoxicity, anti-inflammation, anti-nociceptive and oral ulcer healing properties of coconut shell liquid smoke. *J. Herbmed Pharmacol.* **2021**, *10*, 459–467. [[CrossRef](#)]
25. Montalbano, G.; Molino, G.; Fiorilli, S.; Vitale-Brovarone, C. Synthesis and incorporation of rod-like nano-hydroxyapatite into type I collagen matrix: A hybrid formulation for 3D printing of bone scaffolds. *J. Eur. Ceram Soc.* **2020**, *40*, 3689–3697. [[CrossRef](#)]
26. Abou Neel, E.A.; Aljabo, A.; Strange, A.; Ibrahim, S.; Coathup, M.; Young, A.M.; Bozec, L.; Mudera, V. Demineralization–remineralization dynamics in teeth and bone. *Int. J. Nanomed.* **2016**, *11*, 4743–4763. [[CrossRef](#)]
27. Dey, P. Bone mineralization. In *Contemporary Topics about Phosphorus in Biology and Materials*; Churchill, D.G., Maja Dutour, S., Čolović, B., Füredi Milhofer, H., Eds.; IntechOpen: London, UK, 2020; pp. 1–18.
28. Holzapfel, B.M.; Reichert, J.C.; Schantz, J.T.; Gbureck, U.; Rackwitz, L.; Nöth, U.; Jakob, F.; Rudert, M.; Groll, J.; Hutmacher, D.W. How smart do biomaterials need to be? A translational science and clinical point of view. *Adv. Drug Deliv. Rev.* **2013**, *65*, 581–603. [[CrossRef](#)]
29. de Campos Vidal, B.; Mello, M.L.S. Collagen type I amide I band infrared spectroscopy. *Micron* **2011**, *42*, 283–289. [[CrossRef](#)]
30. Riaz, T.; Zeeshan, R.; Zarif, F.; Ilyas, K.; Muhammad, N.; Safi, S.Z.; Rahim, A.; Rizvi, S.A.; Rehman, I.U. FTIR analysis of natural and synthetic collagen. *Appl. Spectrosc. Rev.* **2018**, *53*, 703–746. [[CrossRef](#)]
31. Ślósarczyk, A.; Paszkiewicz, Z.; Paluszkiwicz, C. FTIR and XRD evaluation of carbonated hydroxyapatite powders synthesized by wet methods. *J. Mol. Struct.* **2005**, *744*, 657–661. [[CrossRef](#)]

32. Chandrasekar, A.; Sagadevan, S.; Dakshnamoorthy, A. Synthesis and characterization of nano-hydroxyapatite (n-HAP) using the wet chemical technique. *Int. J. Phys. Sci.* **2013**, *8*, 1639–1645.
33. Chen, L.; Wu, Z.; Zhou, Y.; Li, L.; Wang, Y.; Wang, Z.; Chen, Y.; Zhang, P. Biomimetic porous collagen/hydroxyapatite scaffold for bone tissue engineering. *J. Appl. Polym. Sci.* **2017**, *134*, 45271. [[CrossRef](#)]
34. Sripriya, R.; Kumar, R. Denudation of human amniotic membrane by a novel process and its characterisations for biomedical applications. *Prog. Biomater.* **2016**, *5*, 161–172. [[CrossRef](#)] [[PubMed](#)]
35. Seckler, M.M.; Danese, M.; Derenzo, S.; Valarelli, J.V.; Giulietti, M.; Rodríguez-Clemente, R. Influence of process conditions on hydroxyapatite crystallinity obtained by direct crystallization. *Mater. Res.* **1999**, *2*, 59–62. [[CrossRef](#)]
36. Huang, Y.; Zhou, G.; Zheng, L.; Liu, H.; Niu, X.; Fan, Y. Micro-/Nano-sized hydroxyapatite directs differentiation of rat bone marrow derived mesenchymal stem cells towards an osteoblast lineage. *Nanoscale* **2012**, *4*, 2484–2490. [[CrossRef](#)]
37. Bal, Z.; Kaito, T.; Korkusuz, F.; Yoshikawa, H. Bone regeneration with hydroxyapatite-based biomaterials. *Emerg. Mater.* **2020**, *3*, 521–544. [[CrossRef](#)]
38. Shukla, S. Freeze drying process: A review. *Int. J. Pharm. Sci. Res.* **2011**, *2*, 3061–3068.
39. Schoof, H.; Apel, J.; Heschel, I.; Rau, G. Control of pore structure and size in freeze-dried collagen sponges. *J. Biomed. Mater. Res.* **2001**, *58*, 352–357. [[CrossRef](#)]
40. Kim, H.W.; Knowles, J.C.; Kim, H.E. Hydroxyapatite and gelatin composite foams processed via novel freeze-drying and crosslinking for use as temporary hard tissue scaffolds. *J. Biomed. Mater. Res. A* **2005**, *72*, 136–145. [[CrossRef](#)]
41. Tohamy, K.M.; Mabrouk, M.; Soliman, I.E.; Beherei, H.H.; Aboelnasr, M.A. Novel alginate/hydroxyethyl cellulose/hydroxyapatite composite scaffold for bone regeneration: In Vitro cell viability and proliferation of human mesenchymal stem cells. *Int. J. Biol. Macromol.* **2018**, *112*, 448–460. [[CrossRef](#)]
42. Angulo, D.E.L.; do Amaral Sobral, P.J. Characterization of gelatin/chitosan scaffold blended with aloe vera and snail mucus for biomedical purpose. *Int. J. Biol. Macromol.* **2016**, *92*, 645–653. [[CrossRef](#)]
43. Danilevicius, P.; Georgiadi, L.; Pateman, C.J.; Claeysens, F.; Chatzinikolaidou, M.; Farsari, M. The effect of porosity on cell ingrowth into accurately defined, laser-made, polylactide-based 3D scaffolds. *Appl. Surf. Sci.* **2015**, *336*, 2–10. [[CrossRef](#)]
44. Zhang, Q.; Jiang, Y.; Zhang, Y.; Ye, Z.; Tan, W.; Lang, M. Effect of porosity on long-term degradation of poly (ϵ -caprolactone) scaffolds and their cellular response. *Polym. Degrad. Stab.* **2013**, *98*, 209–218. [[CrossRef](#)]
45. Torres-Sanchez, C.; Al Mushref, F.R.A.; Norrito, M.; Yendall, K.; Liu, Y.; Conway, P.P. The effect of pore size and porosity on mechanical properties and biological response of porous titanium scaffolds. *Mater. Sci. Eng. C* **2017**, *77*, 219–228. [[CrossRef](#)] [[PubMed](#)]
46. Li, Y.; Sun, S.; Gao, P.; Zhang, M.; Fan, C.; Lu, Q.; Li, C.; Chen, C.; Lin, B.; Jiang, Y. A tough chitosan-alginate porous hydrogel prepared by simple foaming method. *J. Solid State Chem.* **2021**, *294*, 121797. [[CrossRef](#)]